

Quantifying Noise in Optical Tweezers by Allan Variance

Fabian Czerwinski, Andrew C. Richardson, and Lene B. Oddershede

Niels Bohr Institute, University of Copenhagen
Blegdamsvej 17, 2100 København Ø, Denmark

czerwinski@nbi.dk

<http://www.nbi.dk/tweezer>

Abstract: Much effort is put into minimizing noise in optical tweezers experiments because noise and drift can mask fundamental behaviours of, e.g., single molecule assays. Various initiatives have been taken to reduce or eliminate noise but it has been difficult to quantify their effect. We propose to use Allan variance as a simple and efficient method to quantify noise in optical tweezers setups. We apply the method to determine the optimal measurement time, frequency, and detection scheme, and quantify the effect of acoustic noise in the lab. The method can also be used on-the-fly for determining optimal parameters of running experiments.

© 2009 Optical Society of America

OCIS codes: (000.3110) Instruments, apparatus, and components common to the sciences; (000.5490) Probability theory, stochastic processes, and statistics; (030.4280, 110.4280) Noise in imaging systems; (140.7010) Laser trapping; (230.5170) Photodiodes; (120.4800, 350.4800) Optical standards and testing; (350.4855) Optical tweezers or optical manipulation.

References and links

1. K. C. Neuman, and S. M. Block, "Optical trapping," *Rev. Sci. Instrum.* **75**, 2787–2809 (2004).
2. A. Ashkin, J. M. Dziedzic, and T. Yamane, "Optical trapping and manipulation of single cells using infrared laser beams," *Nature* **330**, 769–771 (1987).
3. P. Hansen, V. Bhatia, N. Harrit, and L. B. Oddershede, "Expanding the optical trapping range of gold nanoparticles," *Nano Lett.* **5**, 1937–1942 (2005).
4. L. Bosanac, T. Aabo, P. M. Bendix, and L. B. Oddershede, "Efficient Optical Trapping and Visualization of Silver Nanoparticles," *Nano Lett.* **8**, 1486–1491 (2008).
5. C. Selhuber-Unkel, I. Zins, O. Schubert, C. Sönnichsen, and L. B. Oddershede, "Quantitative optical trapping of single gold nanorods," *Nano Lett.* **8**, 2998–3003 (2008).
6. L. Jauffred, A. C. Richardson, and L. B. Oddershede, "Three-Dimensional Optical Control of Individual Quantum Dots," *Nano Lett.* **8**, 3376–3380 (2008).
7. E. A. Abbondanzieri, W. J. Greenleaf, J. W. Shaevitz, R. Landick, and S. M. Block, "Direct observation of base-pair stepping by RNA polymerase," *Nature* **438**, 460–465 (2005).
8. J. Liphardt, B. Onoa, S. B. Smith, I. Tinoco, and C. Bustamante, "Reversible unfolding of single RNA molecules by mechanical force," *Science* **292**, 733–737 (2001).
9. A. R. Carter, Y. Seol, and T. T. Perkins, "Precision surface-coupled optical-trapping assay with one-basepair resolution," *Biophys. J.* **96**, 2926–2934 (2009).
10. F. Gittes and C. F. Schmidt, "Signals and noise in micromechanical measurements," *Methods Cell. Biol.* **55**, 129–156 (1998).
11. M. Klein, M. Andersson, O. Axner, and E. Fallman, "Dual-trap technique for reduction of low-frequency noise in force measuring optical tweezers," *Appl. Opt.* **46**, 405–412 (2007).
12. D. W. Allan, "Statistics of atomic frequency standards," *Proc. IEEE* **54**, 221–230 (1966).
13. P. Banerjee, A. Chatterjee, and A. Suman, "Determination of Allan deviation of Cesium atomic clock for lower averaging time," *Indian J. Pure Appl. Phys.* **45**, 945–949 (2007).

14. G. M. Gibson, J. Leach, S. Keen, A. J. Wright, and M. J. Padgett, "Measuring the accuracy of particle position and force in optical tweezers using high-speed video microscopy," *Opt. Express* **16**, 14561–14570 (2008).
15. F. Czerwinski and L. B. Oddershede, "Reliable Data-Streaming Software for Photodiode Readout in LABVIEW," in. prep. (2009).
16. K. Berg-Sørensen, L. B. Oddershede, E. L. Florin, and H. Flyvbjerg, "Unintended filtering in a typical photodiode detection system for optical tweezers," *J. Appl. Phys.* **93**, 3167–3176 (2003).
17. L. B. Oddershede, S. Grego, S. Nørrelykke, and K. Berg-Sørensen, "Optical tweezers: probing biological surfaces," *Probe Microsc* **2**, 129–137 (2001).
18. K. Berg-Sørensen and H. Flyvbjerg, "Power spectrum analysis for optical tweezers," *Rev. Sci. Instrum.* **75**, 594–612 (2004).
19. P. M. Hansen, I. Toliç-Nørrelykke, H. Flyvbjerg, and K. Berg-Sørensen, "*tweezercalib 2.1*: Faster version of MATLAB package for precise calibration of optical tweezers," *Comput. Phys. Commun.* **175**, 572–573 (2006).
20. F. Czerwinski, "BeadFluct v1.0," *MatlabCentral* **24196** (2009), <http://www.mathworks.com/matlabcentral/fileexchange/24196>.
21. P. Kartaschoff, *Frequency and Time* (Academic Press, 1978).
22. F. Czerwinski, "allan v1.71," *MatlabCentral* **21727** (2008), <http://www.mathworks.com/matlabcentral/fileexchange/21727>.

1. Introduction

Optical tweezers are created by tightly focusing a laser beam [1], and if focused in all three dimensions a single laser beam can stably trap and manipulate individual objects with sizes ranging from tens of micrometers down to a few nanometers. Objects as diverse as living cells [2], metallic nanoparticles [3, 4, 5], and even quantum dots have been individually trapped [6]. With correct detection schemes the trap can also be utilized to measure forces and distances, typically in the pico-Newton and nanometer regimes. As the technique is nearly non-destructive to biological specimen, it has been successfully used for example to measure forces exerted and distances travelled by individual motor molecules [7], or to unravel structures created by DNA or RNA templates [8]. For such delicate measurements it is extremely important to eliminate as many noise sources as possible. Recently, an optical tweezers setup was reported to have a sensitivity to steps of a length of one DNA basepair (0.34 nm) [9]. Here, drift was compensated by subtracting the motility of a fiducial marker, which was followed by a beam parallel to the trapping laser beam. This solution thus necessitates the use of two parallel laser beams.

Other imaginative solutions to eliminate noise have been invoked, not just in optical tweezers setups but also for other nano-scopic measurement techniques such as atomic force microscopes. For instance air currents have been eliminated by covering the setup, the entire setup has been mounted on a separate foundation, measurements have been conducted in the middle of the night, or, in case of optical trapping, the molecule investigated has been moved away from any surface that might be subject to drift. But how useful and efficient are these efforts? And how does one lab compare to another in terms of noise? In order to answer these questions it is essential to be able to quantify noise.

The dominant approach to quantify noise is typically with a Fourier analysis. The Fourier transformed integrated noise in a predefined bandwidth has been used to judge the impact of some experimental arrangements [10, 11]. However, Fourier analysis lacks the resolution of accumulative noise with a typical band of frequencies smaller than 0.1 Hz. Simply looking at the spectrum of integrated noise can neither be used as a measure of resolution nor of accuracy.

Allan variance has been put forward as a method to quantify noise and it is developed to extrapolate the impact of tiny aberrations at infinity from a finite measurement. It has mostly found use in engineering communities but also in quantification of noise in atomic clocks [12, 13]. In this letter, we show how to use Allan variance analysis as a reliable method to quantify noise stemming from various sources in optical trapping setups. Allan variance was previously used to quantify noise in an optical tweezers setup with the goal of showing that CMOS cameras have sufficient time resolution to be used as particle tracking devices [14].

Here, we significantly extend the use of Allan variance to much larger time scales and by using this method we answer the following questions: What is the optimal time interval to calibrate to achieve the highest accuracy? Which sampling frequency suits the desired experiment best? What is the noise spectrum of commonly used detection systems such as a quadrant photodiode or a position sensitive diode? In which intervals is one type of detector more accurate than the other? What noise does a piezo stage induce? Which effect does the geometry and stability of the measurement chamber have? Can one leave the radio on during measurements? Lastly, should one work during nights, which kind of virtual silence is silent enough?

We provide the tools to apply Allan variance analysis to any possible noise factor in an optical tweezers setup. Furthermore, the method can equally well be used for other types of equipment where it is custom to analyze long time series, e.g. magnetic tweezers or atomic force microscopy.

2. Materials and Methods

The experiment simply consisted of trapping a polystyrene sphere in an aqueous environment. The optical trap was implemented in an inverted microscope (Leica DMIRBE) where the laser beam (Spectra Physics, Nd:YVO₄, 1064 nm) was tightly focused by a water immersion objective (Leica, HCX, 63x, NA=1.20). To eliminate spherical aberrations of the infrared light, the collar of the objective was set to its lowest setting (0.13 mm). The laser was switched on at least an hour prior to experiment to have an optimal pointing stability. The trapping takes place inside a measurement chamber consisting of two glass cover slips (lower one: thickness 0.13–0.16 mm; upper one: 1 mm) separated by one layer of double-sticky tape. The chamber was filled with a dilute solution of polystyrene spheres (Bangs Labs diameter (800 ± 10) nm) in millipore water. The chambers were sealed by vacuum grease to prevent evaporation of liquid during the experiment. The chamber height was measured by laser deflection for all used chambers to be (95 ± 5) μm . Spheres were trapped 40 μm above the lower glass slip to avoid significant interaction with adjacent surfaces [10]. Experiments were carried out at room temperature.

Figure 1 shows the components which were essential for the present study. After the sample, the scattered laser light was focused through a lens onto a photodiode. Data was collected either by a position-sensitive diode (Pacific Silicon Sensor, DL100-7PCBA3) or a quadrant photodiode (Hamamatsu, S5981 Si-PIN). The recorded voltage signal was amplified and low-pass filtered with 100 kHz, before streamed through an acquisition card (National Instruments, PCI-6251) onto a hard drive. Our custom-made data streaming software was programmed in LABVIEW (National Instruments) and uses features of the TDMS-subpackage [15]. It allowed for acquisition with very high acquisition rates and virtually unlimited acquisition duration (tested for 1 kHz up to 2 h, and 22 min for 100 kHz). The program's error-free use has been checked up to acquisition frequencies of 1 MHz. The limitation in acquisition time was due to the increasing file size, not to the program itself.

Analysis was made on adjacent time series consisting of 2^{24} consecutive points. For an acquisition rate of $f_{\text{acq}} = 22$ kHz, corresponding to time series of about 13 min. Apart from filters inherently present in the detection diodes and electronics [16], all additional filtering was applied during data analysis posterior to acquisition. In addition, a video image of the trapped sphere was recorded by a CCD camera (Sony, XC-ES50, 25 Hz). This was to ensure that only a single sphere was in the trap both at the beginning and end of an experiment.

2.1. Calibration

An optical trap exerts a harmonic force on an trapped object, $F = -\kappa x$, where κ is denoted the trap stiffness and x is the deviation from the object's equilibrium position. The goal of

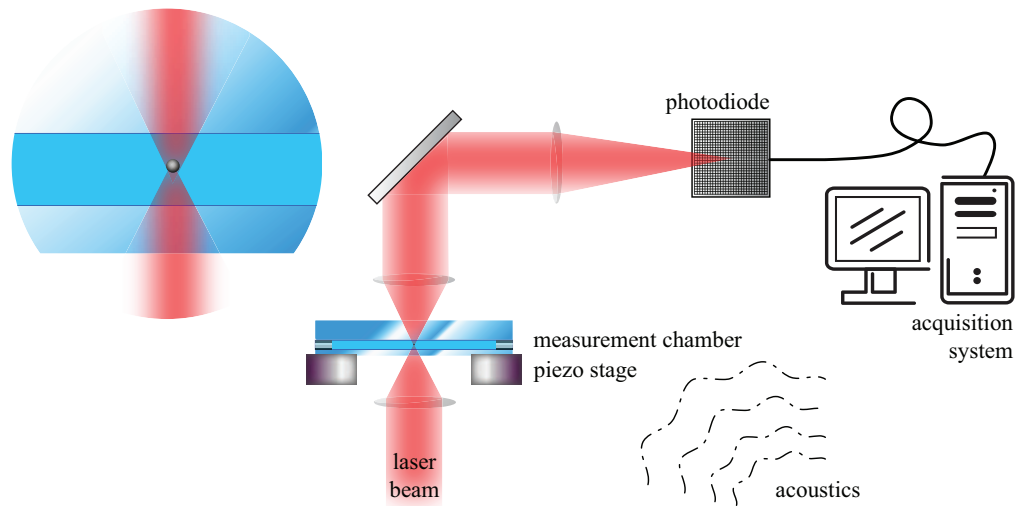


Fig. 1. Schematic drawing of the experimental setup. An infrared laser beam was focused into a sealed measurement chamber which was mounted onto a piezo stage. A polystyrene sphere was trapped in the middle of the measurement chamber which was filled with water (zoom in). The scatter light was collected onto a photodiode. The positional signal of the sphere inside the trap was streamed onto a hard drive. Acoustic noise might have interfered with the experiment.

the calibration procedure is to extract κ which completely characterizes the thermal motion of the trapped object. The equation of motion is well described by the Langevin equation, and a Fourier transformation yields the positional power spectrum, from which the ratio between the trap stiffness and the friction coefficient γ can be found [10]. This ratio is denoted the corner frequency f_c :

$$f_c = \frac{\kappa}{2\pi\gamma}. \quad (1)$$

If a sphere is trapped far away from any surfaces, γ is given by Stokes law: $\gamma = 6\pi\eta r$, where η the viscosity of water ($\eta = 8.9 \cdot 10^{-4}$ sPa), and r the radius of the sphere. The power spectral analysis also provides information regarding the conversion factor β which converts the position measured in volts by the photodiodes to position travelled in nanometers by the trapped sphere [17].

In order to find the correct time interval for the calibration time series we first calculated the Allan variance. For our measurements the absolute minimum of the Allan variance typically occurred around a measurement time in the order of a few seconds, as will be detailed around the description of Fig. 3. Thus, for an acquisition frequency of $f_{\text{acq}}=22$ kHz, we used 2^{16} data points for one individual calibration. Calibration was performed by the power-spectrum method as described in [18] using the program from Ref. [19]. Ten individual calibrations from a longer time series were used to calculate the corner frequency and the conversion factor.

Fourier transformation allows for a reliable, simple, and quick way of calibrating measurements in optical tweezers on-the-fly. In addition, it is particularly useful to pinpoint high-frequency noise. The clear distinct peak in the power spectrum can typically be tracked down to a noise source and eliminated directly. However, when considering only the very low frequency part, assumptions must be made about the drift [11]. Additionally, the typical frequency resolution is simply not good enough. One way to quantify accumulative noise over a broader

frequency band is to look at the integrated noise spectrum [9]. For this one has to assume for instance the boundaries of the integration interval.

2.2. Monte-Carlo Simulations

To compare the experimentally measured time series to values expected for systems that are not exposed to drift, we developed a Monte-Carlo simulation [20]. It calculated the position of micron-sized spheres in an optical trap in meters. The positions of the sphere were drawn with a spacing of numbers of $2.22 \cdot 10^{-16}$. The radius of the sphere r , the corner frequency f_c , the trapping stiffness κ , the acquisition frequency f_{acq} , and the number of sampled points N could be varied. Adjacent time series gained by simulations were treated as regular data and compared to experimental results.

2.3. Allan Variance

For purely stochastic fluctuations which are frequency independent and thus can be used for calibration in atomic clocks or optical tweezers, classical variances usually do not converge. This leads to situations where for example changes to the position due to drift are hidden inside the fluctuating signal. Allan variances have been developed as a consequence of the need of precise atomic and molecular measurements to reveal low- and very-low frequency drift phenomena [21]. It was designed to extrapolate the drift of a system at infinity from finite measurements. Allan variance converges to a finite value for all external noise classically found in nature: Drift (as accumulative noise with $1/f$ -characteristics), shot noise, damped oscillations, etc.

Definition. Given a time series of N elements and a total measurement time of $t_{\text{acq}} = f_{\text{acq}}N$, then Allan variance is defined as:

$$\sigma_x^2(\tau) = \frac{1}{2} \left\langle (x_{i+1} - x_i)^2 \right\rangle_\tau \quad (2)$$

with x_i being the mean over a time interval of a length $\tau = f_{\text{acq}}m$, m the number of elements in this particular interval. $\langle \dots \rangle$ denotes the arithmetic mean. In words, the Allan variance is half the averaged squared mean of neighboring intervals. Consequently, Allan variance can only be calculated for $\tau \leq t_{\text{acq}}/2$, and it is always ≥ 0 . Using $\tilde{x} = \beta x$, the linearity of the Allan variance follows directly from Eq. (2):

$$\sigma_{\tilde{x}}^2(\tau) = \frac{1}{2} \left\langle (\tilde{x}_{i+1} - \tilde{x}_i)^2 \right\rangle = \beta^2 \sigma_x^2(\tau). \quad (3)$$

Therefore, the conversion of Allan variance from arbitrary units to e.g. meters could be done at any time, posterior to calibration for instance.

The statistical error is defined as the standard error of the mean of Eq. (2):

$$\text{SE}_{\sigma(\tau)} = \frac{\sigma_x(\tau)}{\sqrt{n}} = \sqrt{\frac{m}{N}} \sigma_x(\tau) = \sqrt{\frac{\tau}{t_{\text{acq}}}} \sigma_x(\tau). \quad (4)$$

This is valid for $\tau \ll t_{\text{acq}}$. For $\tau < t_{\text{acq}}$, $\text{SE}_{\sigma(\tau)}$ can be approximated by utilizing $n \approx \lfloor N/m \rfloor = \lfloor t_{\text{acq}}/\tau \rfloor$. Note, in this definition the neighboring time intervals of length τ are in principle conditionally independent. When τ is on the order of t_{acq} one faces the problem of low statistics.

Overlapping Allan Variance. To account for the huge statistical error of the Allan variance, Eq. (4), in case of large τ , one can give up the statistical independence of time intervals and use a sliding interval instead. One calculates the difference of two neighboring intervals each containing m elements. Then the intervals move one element further in time while both intervals

lose their ‘oldest’ element, conserving their number of elements. Consequently, the statistical error scales with $1/\sqrt{m(n-1)}$ instead of $1/\sqrt{n}$ as in Eq. (4), the conditionally independent case.

Normal variance. Often, the standard way to calculate variance as the square of the standard deviation of the mean with a sliding window averaging over τ has been used to evaluate drift in a data set with mean \bar{x} :

$$\sigma^2(\tau) = \frac{1}{2} \left\langle (x_i - \bar{x})^2 \right\rangle_{\tau}. \quad (5)$$

However, one problem of this normal variance is that it does not converge for noise regularly occurring in nature, e.g. white noise.

2.4. Thermal Limit

The standard error of an averaged position of an object can be used to access its limit for positional detection. It depends only on its diffusion $\langle x^2 \rangle = 2D\tau$ with the diffusion constant $D = k_B T / \gamma$. It can be further confined by a trapping potential characterized by a trapping constant κ . Using the same approximation as for Eq. (4), the statistical error for a trapped sphere becomes:

$$SE_{\langle x \rangle} = \frac{1}{\sqrt{n}} \sqrt{\langle x^2 \rangle} \approx \sqrt{\frac{2k_B T \gamma}{\kappa^2 \tau}}. \quad (6)$$

This limit cannot be beaten by any measurement that does not oversample a desired signal. In the following the Allan variances found are compared to this thermal limit. In the case of dual optical traps the expression is slightly changed [11].

2.5. Allan Variance for Optical Tweezers Setups

To analyze data from experiments with optical tweezers a set of requirements has to be fulfilled. To access a broad range of possible values for time intervals τ , one of the requirements is a device which allows for an acquisition of positional data at a fast and a reliable rate over a (very) long measurement time.

Allan variances of position time series of a trapped polystyrene sphere were calculated by using a custom-made MATLAB program [22]. The program calculated time-stamped as well as time varying data. In the case of time-stamped data, vectorization of the interval used for mean and difference calculations allow for very fast calculation of the Allan variance even for our longest data sets.

We tested the impact of various parameters, e.g. acoustic noise, sample stability, geometry, and photodiodes by doing a set of three time series (typically at $f_{\text{acq}} = 22$ kHz for about 13 min, i.e. 2^{24} data points for each coordinate). Then we altered the parameters and repeated the measurements. Though the Figs. of the results section represent plots of particular datasets, all experiments have been repeated as described above and all results explicitly stated are solid and reproducible. We found it advantageous to plot Allan variances in log-log plots. In those, slopes correspond to the exponent of a proposed relation.

3. Results

Using the optical tweezers setup we measured time series of a sphere’s position and using Monte-Carlo simulations we created time series of the same length using the same physical parameters. One important difference between the experimental data points and the simulation was that the experimental data were subject to various sources of noise, e.g. long term drift. There were no such noise terms in the simulated data. Figure 2(a) shows the position versus time of an optically trapped polystyrene sphere, green line shows experimental results, light grey line

simulated data. (b) shows position histograms of two complete time series $N = 262,144$ which overlap precisely. In (c) the positional power spectral density of the two data sets are plotted, the full lines show Lorentzian fits to the power spectra. These fits include the effect of aliasing and for the experimental data the filtering effect of the photodetection system and electronics as implemented in the software [19]. The full black line is a fit to experimental data, and the light grey one is fitted to simulated data. The point where the curve crosses from being horizontal to having a slope of -2 is denoted the corner frequency f_c [18]. It is directly proportional to the trap stiffness κ (Eq. (1)). At high frequencies one sees that the well understood effect of photodiode filtering [16] causes the experimental data to lie beneath the simulated data, which are 'only' subject to aliasing [18]. Drift, which is inherently present in the experimental but not in the simulated data, does not show, not even at the low frequency end.

3.1. Allan Variance for Individual Experiments

The Allan variance was calculated from the time series using Eq. (2), for the example shown in Fig. 3 where the original time series spanned about 13 min. The green curves are from an experiment where a polystyrene sphere with a diameter of 800 nm was trapped with a corner frequency of 800 Hz, hence $\kappa = 33.6$ pN/ μm . The green-grey curves stem from a Monte-Carlo simulation. The orange curves are from an experiment with a stronger trap, $f_c=1600$ Hz, $\kappa = 67.7$ pN/ μm . The orange-grey curves are from the corresponding simulation. The full lines denote the overlapping Allan variance. Due to its improved statistics, it is always inside the variation of the Allan variance. This is particularly evident for large τ .

The dashed lines with a slope of $-1/2$ are the thermal limits for those two trapping stiffnesses according to Eq. (6). For short time intervals, all Allan variances fall below the thermal limit because adjacent positions are correlated. The absolute maxima of the Allan variance can be found at $\pi\tau_c = (2f_c)^{-1}$. The inset of Fig. 3 shows the autocorrelation time, orange is for the strong trap, green for the weaker one. For $\tau > 2\pi/(2f_c) = 2\pi^2\tau_c$, Allan variances are above the respective thermal limits and decay with a characteristic slope of $-1/2$ for a wide range of measurement times. The fact that the Allan variance stays very close to the thermal limit is a benchmark of an extremely stable setup. The deviation from the thermal limit beyond 1 s is due to drift, as the comparison between simulated and experimental data illustrates. The Allan variance reaches a global minimum for measurement times in the range of seconds. This is the timespan which denotes the optimal measurement time for calibrations. Here one finds a balance between a time long enough allowing for the Gaussian distributed parameters to be accurately determined and a time short enough that drift does not yet play a significant role. This optimal measurement time depends on the trap stiffness. As expected, a stronger trap ensures a smaller Allan variance than a weaker trap, which implies a higher positional accuracy. This is particularly true for long time scales. The normal variance is also plotted in Fig. 3 using dotted lines.

3.2. Accuracy Depends on Acquisition Frequency

Another question which was addressed by Allan variance analysis was the question of optimal acquisition frequency f_{acq} . A polystyrene sphere was optically trapped and the data acquisition frequency was varied between 10 Hz and 100 kHz. The result of the corresponding overlapping Allan variance is shown in Fig. 4.

In Fig. 4(a), the graphs have the same characteristic trajectories as those shown in Fig. 3, but it is apparent that the Allan variance decreases with higher acquisition frequency up to a certain threshold. This threshold is the inverse correlation time τ_c^{-1} and depends on the trapping stiffness. It can be found in the plotted data set at $\tau_c^{-1} = 2\pi f_c \approx 10$ kHz. Above this threshold, an increase in frequency does not change the Allan variance for the majority of the measure-

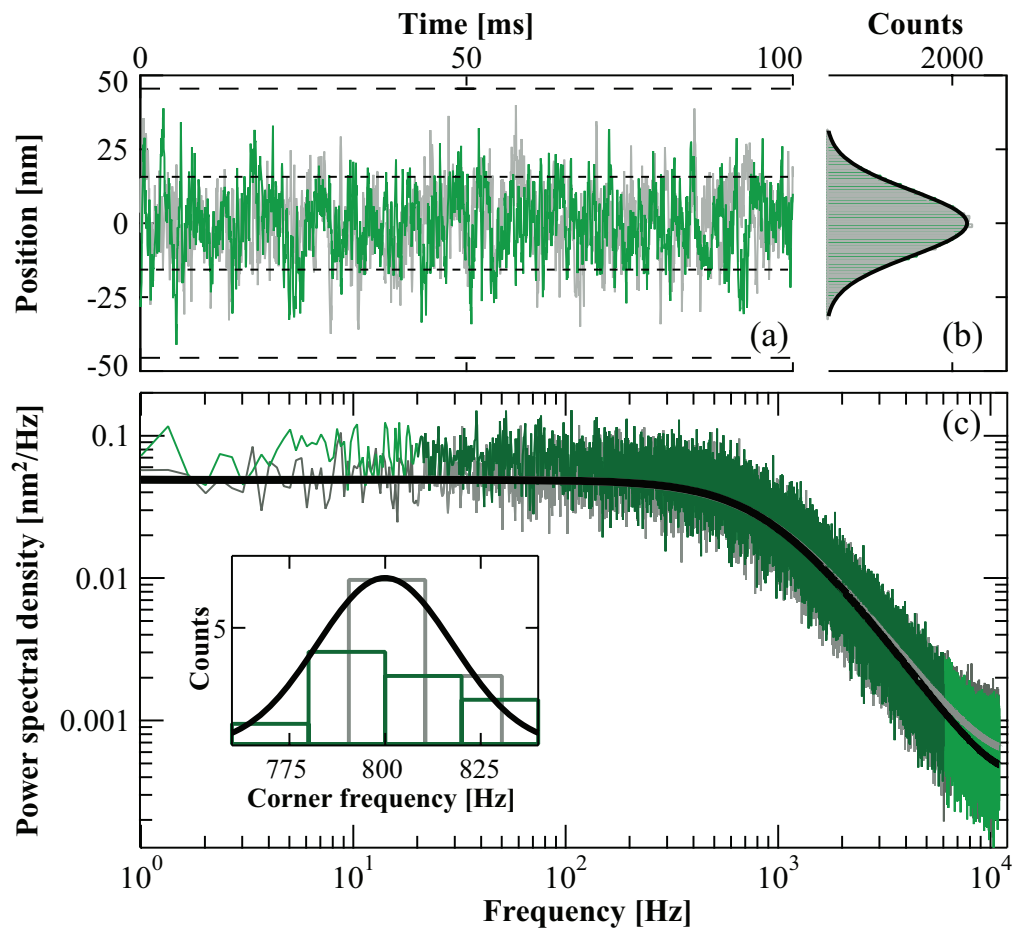


Fig. 2. (a) Experimental (green) and simulated (grey) position time series of an optically-trapped polystyrene sphere in water. The traces are centered around 0 nm, and the dashed lines indicate the interval $\pm\sigma$, respectively $\pm 3\sigma$. (b) Variance σ is obtained by fitting a Gaussian to the overlapping positional histogram. (c) The power spectral density of experimental (green) and simulated (grey) positional sequences. Each graph is the average of 10 individually calculated power spectra for traces of about 3 s. The band from 20 to 6000 Hz was used to obtain corrected Lorentzian fits (experimental: black; simulation: grey). The inset shows the spread in corner frequencies from individual calibrations. This spread follows a Gaussian distribution.

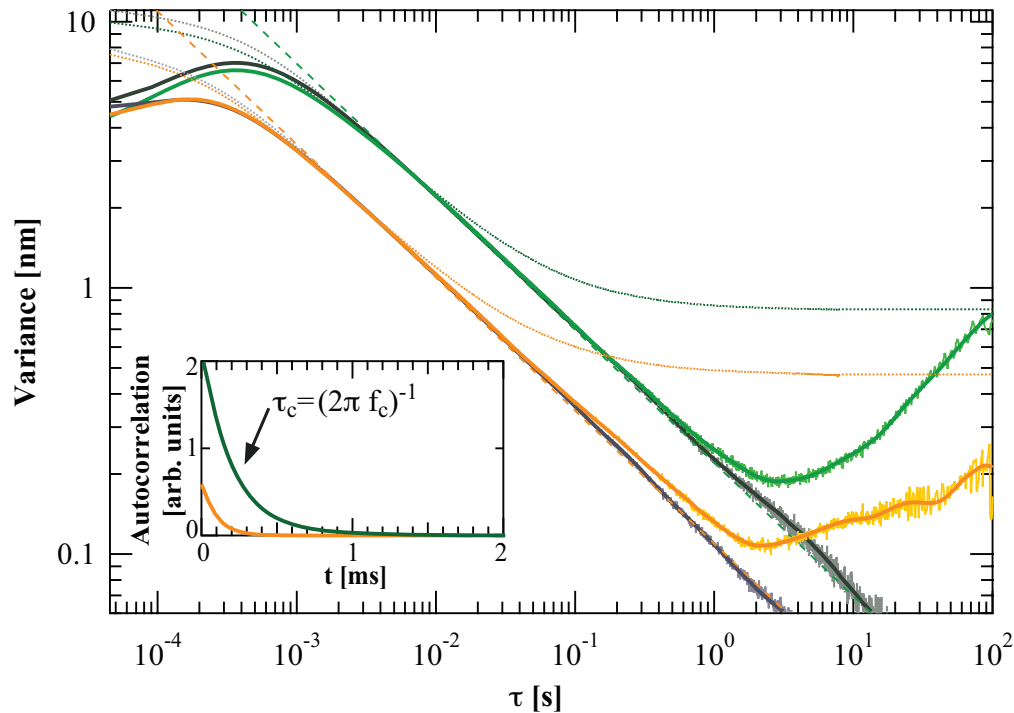


Fig. 3. Variances of individual optical tweezers experiments. The variances were calculated from the position of a polystyrene sphere trapped with $\kappa = 67.7 \text{ pN}/\mu\text{m}$ (orange) or with $\kappa = 33.6 \text{ pN}/\mu\text{m}$ (green). Grey graphs show results of Monte-Carlo simulations using the same physical parameters. Dashed lines are the thermal limits according to Eq. (6). The dotted lines are graphs of the normal variances using Eq. (5). Remarkably, the Allan variance provides half an order of magnitude higher sensitivity for $\tau > 1 \text{ s}$.

ment times. Only above the optimal interval, around 10 s, it seems beneficial to improve the acquisition frequency above 10 kHz. However, the bandwidth of the used position-sensitive photodiode was found to lie in between 43 and 47 kHz. Hence, the apparent aliasing might be the reason for the steeper slope for measurement times $\tau > 20 \text{ s}$ in the plotted graphs.

Figure 4(b) shows the result of rescaling the measurement time onto the number of acquired data points. The Allan variance changes with the number of acquired data points for various sampling frequencies. Hence, for a high acquisition rate the number of data points needs to be large in order to achieve highest accuracy. In principle, this can be used to extract information regarding how much extra precision is gained by acquiring additional data points. Furthermore, the difference of the graphs from the 'line of maximum information' indicates how much information a data point at the given acquisition frequency contains. For acquisition frequencies $f_{\text{acq}} < \tau_c^{-1}$ one measures thermal fluctuations of the sphere without any informational content.

3.3. Acoustics and Chamber Geometry

We also investigated the effect of acoustic noise in the lab. Two different situations were compared: (i) A silent lab early Saturday morning where efforts were made to shield the equipment from noise. And (ii) a lab with more acoustic noise under everyday laboratory conditions, e.g., other people working the the lab and talking, the radio on, the equipment was not covered and

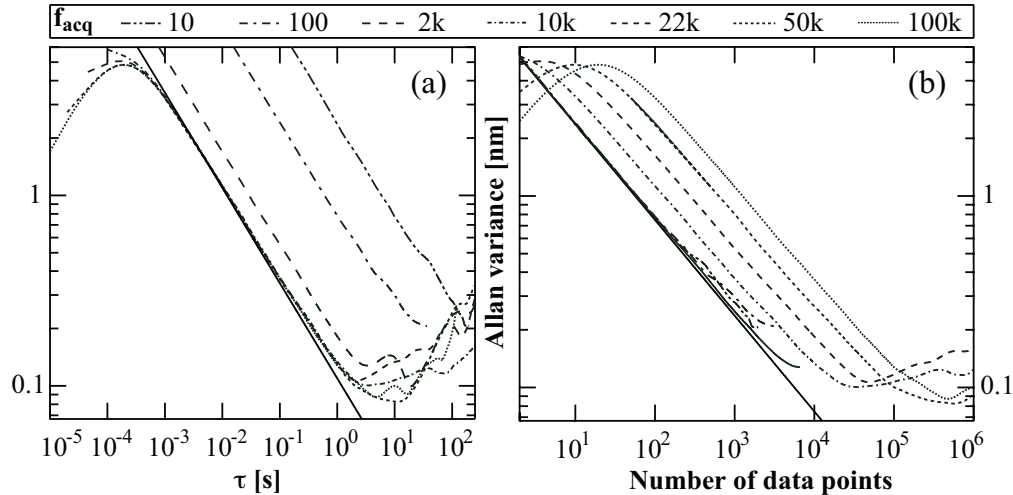


Fig. 4. Allan variance depends on the acquisition frequency (a) and on the number of data points (b). Each time series had a length of about 13 min, the acquisition frequency f_{acq} was varied, and the trap stiffness was $\kappa = 67.7 \text{ pN}/\mu\text{m}$.

ambient light would also enter the photo detection system. Figure 5 shows the measurements of Allan variance under those two conditions. The full lines are Allan variances of experimental data from an optically trapped sphere under virtual silence (i), and the dash-dotted lines are from noisy conditions (ii).

The aqueous sample chamber was asymmetric with inner dimensions 5 cm (x), 1 cm (y), and $95 \mu\text{m}$ (z) and the sphere was trapped approximately in the center of this chamber. The green traces in Fig. 5 are Allan variances of the adjacent time series in x , the red traces those of y . The black full lines denote the thermal limit. The measurement chamber was sealed with a thin glass cover slip at the bottom towards the focusing objective and at the top either a thick cover slip (1 mm, data in Fig. 5(a)) or a thin cover slip (0.13–0.16 mm, data in Fig. 5(b)).

Figure 5 shows that the effect on the Allan variance of reducing acoustic noise is minimal on the y -direction, the smallest lateral dimension of the chamber. However, in the x -direction, the longest lateral direction of the chamber, there is a significant effect of reducing acoustic noise. To check the directional dependence of these results we rotated the chamber 90° and still saw the effect. In other words, the difference in x and y directions are due to sample geometry and not to asymmetries in the laser or detection system. All other plots of Allan variances in the present letter originate from the longest direction in an elongated chamber (corresponding to the x -direction in Fig. 5).

Making the chamber with a thick rather than a thin cover slip at the top stabilizes the chamber for all sampling times above $\sim 0.3 \text{ s}$. This can be seen by comparing Figs. 5(a) and 5(b). To facilitate the comparison a grey horizontal line is drawn at 0.17 nm accuracy in both plots. Another effect emerging from using different upper cover slips is the different scaling properties of the Allan variance at long measurement times. Full lines with slopes of 1 in (a) and $1/2$ in (b) are drawn in the Fig. 5 to facilitate the comparison of the scaling trends of the Allan variance for $\tau > 20 \text{ s}$.

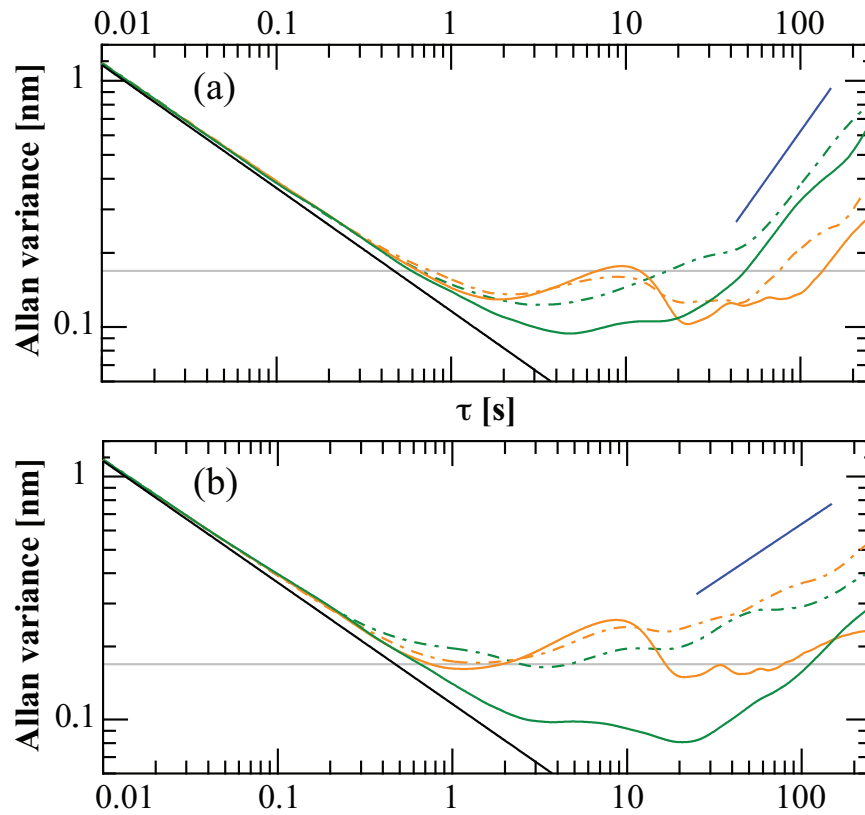


Fig. 5. Impact of measurement-chamber construction and acoustic noise in the laboratory. (a) Allan variance for the position of a trapped sphere, $\kappa = 53.4 \text{ pN}/\mu\text{m}$. x (green) is the longest lateral dimension of the measurement chamber. Accordingly, y (orange) denotes the shortest lateral dimension. The upper cover slip has a thickness of 1 mm. Solid lines are measured in virtual silence, dash-dotted lines are measured with acoustic noise in the laboratory. (b) Same conditions as in (a), but using an upper cover slip of a thickness of 0.13–0.16 mm. The solid black curves represent the thermal limit and grey line is a guide to the eye at 0.17 nm. The blue lines indicate the slope for low-frequency drift, 1 for (a) and 1/2 for (b).

3.4. Piezo Stage

Many optical tweezers experiments involve the usage of a piezo stage. It might be possible that mounting the sample on a piezo stage induces additional noise. To investigate this we performed an experiment where a sphere was optically trapped and its Allan variance was calculated both for the situation where the piezo stage was turned on and where it was off. Figure 6 shows the Allan variance of a trapped sphere, $\kappa = 33.6 \text{ pN}/\mu\text{m}$ (violet) with the piezo on. When decreasing the trap stiffness to $\kappa = 15.3 \text{ pN}/\mu\text{m}$ (red), the loss in accuracy over measurement intervals of $0.5 \text{ s} < \tau < 110 \text{ s}$ became even more pronounced; whereas switching off the piezo and keeping the trap stiffness constant at $\kappa = 15.3 \text{ pN}/\mu\text{m}$ (green) eliminated the effect. Hence, the piezo does add noise to the system, in particular in a measurement time interval $0.5 \text{ s} < \tau < 110 \text{ s}$. Furthermore, Fig. 6 confirms the findings from Fig. 3 that stronger traps can partially eliminate low-frequency noise. The black trace shown in Fig. 6 is the Allan variance of the output of the control box yielding the position of the piezo while the sample was mounted. For short measurement times, the Allan variance shows local maxima that correspond to odd-numbered divisors of the piezo's resonance frequency. The resonance of the piezo has thus not been altered significantly by mounting the stage. At measurement times within $0.5 \text{ s} < \tau < 110 \text{ s}$, the noise of the stage alone peaks in the same interval as the noise peak in the violet and red curves. Therefore, we propose that the piezo stage contributes to the noise as quantified by Allan variance in a frequency interval as visualized by the grey shading in Fig. 6. Those low-frequency phenomena would be challenging to identify using standard noise-detection methods.

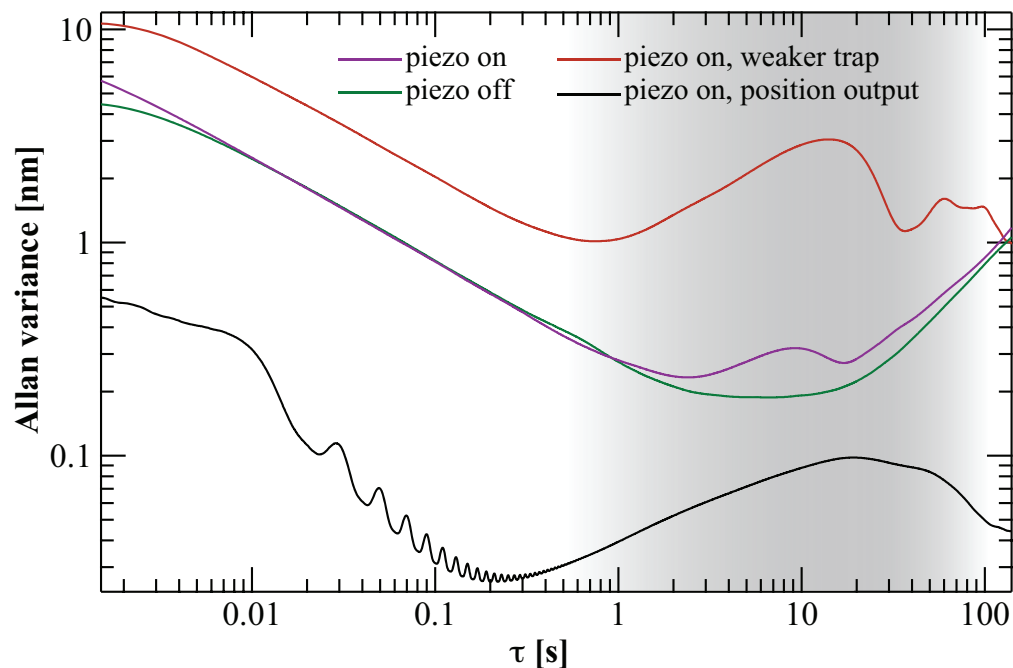


Fig. 6. Impact of piezo stage on Allan variance for a trapped sphere. When the piezo is switched on a hill in the Allan variance within the interval $0.5 \text{ s} < \tau < 110 \text{ s}$ is observed (grey shading). It is more pronounced for a weaker trapped sphere, $\kappa = 15.3 \text{ pN}/\mu\text{m}$ (red), than for a strongly trapped sphere, $\kappa = 33.6 \text{ pN}/\mu\text{m}$ (violet). The Allan variance of the piezo itself is plotted in black. When the piezo is switched off (green), the hill disappears.

3.5. Comparison of Photodiodes

One further issue which was investigated by Allan variance analysis was the noise contribution from different types of photodiode-based detection systems, from the laser, and the data acquisition electronics. These effects are visualized in Fig. 7: The full lines show Allan variances of a trapped polystyrene sphere, $\kappa = 33.6 \text{ pN}/\mu\text{m}$, using either the position-sensitive diode (PSD, green) or the quadrant photodiode (QPD, orange). It was the same sphere trapped in both cases. The performances of the two types of photodiodes were quite similar, but for the shortest as well as for the longest measurement times the PSD had a smaller Allan variance. Another experiment was performed where there was nothing inside the optical trap, but the laser was shining directly at the photo detection system. An optically trapped sphere has a focusing effect on the laser light, so in the absence of a trapped sphere the total signal on the detection system is significantly smaller than when a sphere is trapped using the same laser intensity. The dashed lines in Fig. 7 show the Allan variance of the laser signal as detected by the QPD (orange) and PSD (green), respectively. Generally, the noise of the PSD is lower than of the QPD. Interestingly, one sees a pronounced peak in the Allan variance of the QPD around 16 ms. This time interval corresponds exactly to the detection delay time reported for this particular diode [16]. The black dotted line is the Allan variance of the electric noise from the acquisition system, in this experiment the PSD was on, but the laser was off. The dash-dotted horizontal line in Fig. 7 denotes the resolution of the acquisition system.

4. Discussion

Allan variance is a strong tool to quantify noise in optical tweezers setups. However, it is advantageous to combine it with Fourier analysis. The Fourier transformation of a positional time series is conveniently used for calibration and is efficient to identify noise that occurs at high frequencies, typically above 1 Hz. Nonetheless, Fourier analysis lacks resolution for noise with characteristic frequencies lower than approximately 1 Hz. In particular an accumulative low-frequency noise as drift is almost impossible to identify. One should also be aware that for a method which considers the integrated noise one limitation is that it strongly depends on the choice of bandwidth. The normal variances go towards an asymptotic value which denotes the positional variance of the trap, but Allan variances can probe way below this limit. The reason can be found in the convergence of the Allan variance for most of the naturally occurring types of noise, whereas a normal variance does not converge for purely stochastic noise. Thus, a normal variance carries no information about, e.g. the optimal measurement time for calibrations.

In our experiments Allan variance analysis has revealed that, if a sampling frequency of 22 kHz and typical trap stiffnesses of 10–140 pN/ μm are used, the optimal length of a time series for calibration is in the order of seconds, not e.g. tens of seconds. This time scale is on the same order as reported in [14]. Still, our Allan variance is closer to the thermal limit than those reported for a similar setup in [14]. This finding emphasizes the stability of our setup. This comparison also shows one strength of the Allan variance analysis, namely to compare different labs, different setups, or different settings with respect to noise contributions.

One should note, that when investigating other measures than just positions, one might need to construct an adapted Allan variance. An example can be found in [14] where an Allan variance for force measurements is derived. Notably, these may show the higher force accuracy and time stability for weaker traps.

Interestingly, we found a pronounced dependence of the Allan variance on chamber geometry and on whether the measurement chamber had been stabilized with a thicker cover slip. Thicker cover slips decrease the Allan variance, up to measurement times in the order of hundreds of seconds. However, beyond those we found steeper slopes for thick cover slips. As thick cover slips were meant to stabilize measurements made in microscopes over all timespans, this

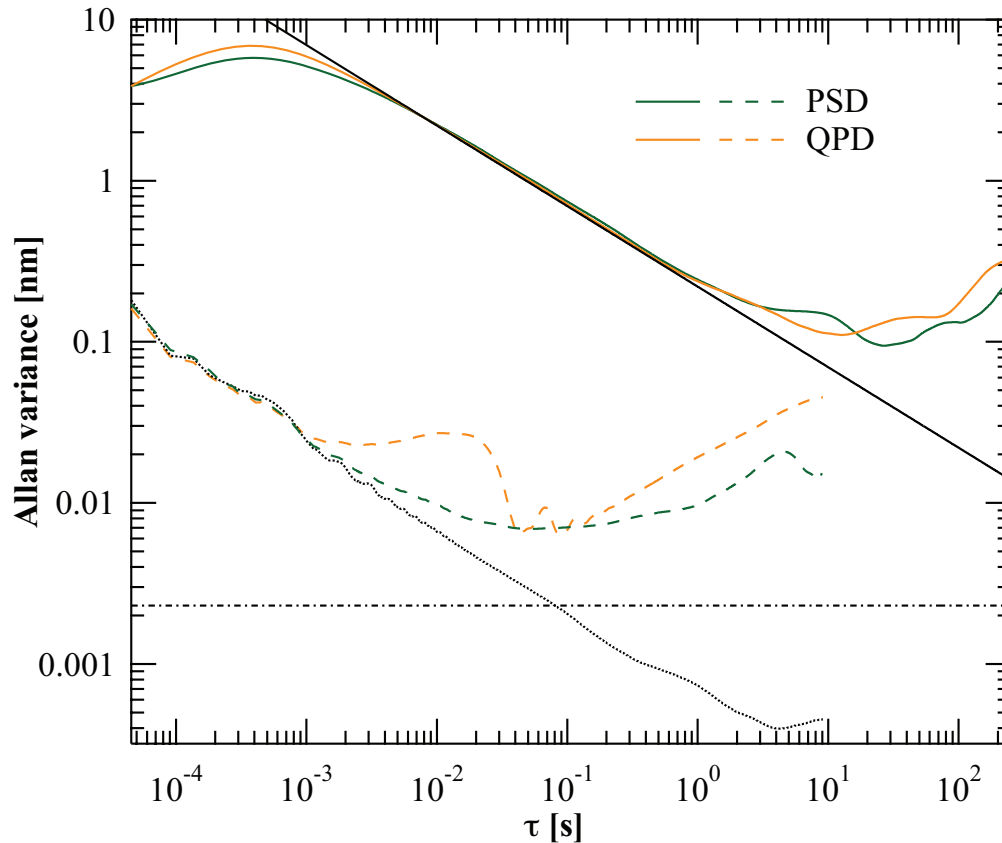


Fig. 7. Effect of photodiodes on Allan variance, PSD (green) and QPD (orange), $\kappa = 33.6 \text{ pN}/\mu\text{m}$. The solid black line gives the thermal limit. The dashed lines mark the Allan variance when the diodes are shined on by the laser with nothing trapped. The dotted line marks the purely electronic noise when every illumination was blocked. It drops below the best resolution possible for the given photodiode-based detection system with the used acquisition settings (dash-dotted line).

was unexpected. Here again, Allan variance analysis revealed and quantified a low-frequency drift phenomena which would not have been visible by the normal variance. For the chamber geometry, the shortest direction of the chamber was subject to significantly more noise than the longer direction. The origin of this geometry dependence is subject to future investigations. Elimination of acoustic noise does not significantly decrease the Allan variance, in particular not along the shortest direction of the sample chamber. Hence, one can safely tune into one's favorite radio station and operate experiments during regular working hours.

Optical tweezers setups are often equipped with photodiode detection systems and the chamber often mounted on a piezo stage. Both the photodiode and the piezo stage contribute to the total noise spectrum of the system, so if the piezo stage is not necessarily needed for a particular experiment, it would be advantageous to switch it off. Allan variance is not a measure of resolution, but rather of accuracy. One would have to put a signal of a known input into the system and monitor its output to obtain a measure of the resolution. For such experiments one typically uses a piezo stage to move a stuck sphere in a controlled fashion. But, as piezo systems are exposed to fluctuations and drift, resolution inputs should therefore be chosen where

the fluctuations of the piezo stage have the smallest Allan variance.

A comparison of the performance of a quadrant photodiode to the performance of a position sensitive diode showed that they were nearly performing identically. Nevertheless, both for very short and very long measurement times the position sensitive diode was performing slightly better. Moreover, we saw the footprint of the 3 dB filtering frequency of the quadrant photodiode around 16 ms as expected [16].

Allan variance seems to be a straight forward method to quantify noise in optical trapping assays. One reason why it has not been established before could be the necessary software implementations because one has to work with very large datasets. To our knowledge, only one publication [14] previously took advantage of this method, even though they limited their analysis to data sets of 300,000 points taken over 5 min. Our software solutions capable of handling significantly larger datasets are freely available through the MATLABCentral.

Our results showed that optical tweezers have a resolution close to the thermal limit for measurement times between 100 ms and 100 s. This is precisely the interval where most of the biological processes like molecular motors typically have been tested with optical tweezers. Thus, Allan variance analysis might strengthen these experiments against criticism regarding drift sensitivity. With the tools described in this letter this type of analysis can be done on-the-fly along with regular experiments.

5. Conclusions

We have used Allan variance as a method to quantify noise in a force-measuring optical tweezers setup over more than 6 decades in time. The noise which is pinpointed by this method is difficult or impossible to quantify by other methods such as power spectral analysis or normal variance analysis. Through Allan variance analysis we determined the optimal measurement time to achieve a calibration with highest accuracy, as well as the optimal sampling frequency. Allan variance analysis has also shown that the measurement chamber stability as well as its geometry influences the noise spectrum. Typically, chambers for optical trapping experiments are mounted on a piezo stage and data are acquired by photodiodes. We quantified the magnitude and typical interval of noise contribution from these pieces of equipment, thus making it possible for example to perform a qualified choice between which type of diode to use for a particular experiment. In principle, this type of analysis can be used in any kind of single-molecule technique where it is advantageous to quantify and possibly eliminate or minimize noise sources. It can easily be used as a complimentary technique, in addition to Fourier analysis, as a standard method of comparing different laboratories and their performance.

Acknowledgements

We acknowledge discussions with and inputs from M. Andersson, P. M. Bendix, K. Berg-Sørensen, P. Gerlee, U. F. Keyser, M. Mahamdeh, S. A. Mir, R. Seidel, and D. Stein. The project was financially supported by the Excellence program of the University of Copenhagen, and the Marie Curie Grant MP6-MEST-2004-504465.